CONTROL STRATEGIES FOR TIMESTEP SELECTION AND CONVERGENCE RATE OF NONLINEAR ITERATIONS IN SIMULATION OF RAYLEIGH-BENARD-MARANGONI FLOWS

Andréa M. P. Valli*, Álvaro L. G. A. Coutinho† and Graham F. Carey ‡

* Department of Computer Science
Federal University of Esp. Santo, Brazil
Av. F. Ferrari S/N - CEP 29069-900 - Vitória - ES, Brazil
e–mail: avalli@inf.ufes.br

† Civil Engineering Department
COPPE/Federal University of Rio de Janeiro, Brazil
P.O. Box 68506 - CEP 21945-970 - Rio de Janeiro, RJ, Brazil
e–mail: alvaro@coc.ufrj.br

‡ Department of Aerospace and Engineering Mechanics
The University of Texas at Austin, USA
ASE/EM Dept., WRW 301, Austin, TX 78712, USA
e–mail: carey@cfdlab.ae.utexas.edu

Key Words: Adaptive Timestep Control, Nonlinear Iterations, Finite Element, Rayleigh-Benard-Marangoni Flows

Abstract. *This work investigates the use of control strategies for timestep selection and convergence rate improvement of nonlinear iterative processes in the finite element solution of 2D viscous flows problems involving heat transfer combined with surface tension effects. The present solution method employs a decoupled scheme, where the finite flow formulation is based on a penalty Galerkin method and the heat transfer computations use a Galerkin formulation. We compare the efficiency of the control strategies for timestep selection with another heuristic adaptive stepsize selection scheme. Numerical results for representative Rayleigh-Benard-Marangoni problem confirm that the non-dimensional kinetic energy could be a suitable parameter to improve the timestep selection when coordinate with the convergence rate control of the nonlinear iterations.*

1 INTRODUCTION

When a thin horizontal layer fluid between two horizontal plates is heated from below, a temperature gradient is generated across the plates. At a critical Rayleigh number, circular convection cells set in - the heated fluid near the bottom begins to rise while the cooler fluid near the top descends. Buoyancy is a dominant component in driving this type of flow termed Rayleigh-Benard problem. If the plate is removed from the upper surface, then the surface tension effects associated with temperature gradients on the free surface become important. Now both buoyancy and thermocapillary effects provide the dominant forces driving the flow for this classical Rayleigh-Benard-Marangoni problem.

To develop effective algorithms capable of high resolution transient flow and heat transfer computations, we need improved techniques. For example, domain decomposition strategies and parallel gradient-type iterative solution schemes have been developed and implemented with success for 3-D Rayleigh-Benard-Marangoni flow calculations.[1] These techniques permit making fundamental phenomenological flow studies at the grid resolution necessary to represent the fine scale surface-driven phenomena. Also, with the evolution of the methodology and its extension to more complex classes of coupled problems, there has been an increasing need for other enhancements such as adaptive grid refinement and coarsening. Several adaptive timestepping selection strategies have been studied as a means to provide stable accurate transient (and steady state) solutions more efficiently.[2–6]

In the numerical integration of ordinary differential equations by implicit timestepping methods, a system of nonlinear equations has to be solved at every step. In general, it is common to use fixed-point iterations or modified Newton iterations. In the present work, we use fixed-point iterations given by successive approximations. The convergence rate of the iterative methods depends on the stepsize,[7] and the computational efficiency of the method can be measured by the total number of successive iterations to obtain the final solution. To improve efficiency, diminishing computational costs, it is necessary to control the convergence rate of the fixed point iterations.

The focus in our work is the use of control strategies for timestep selection and convergence rate improvement of nonlinear iterative processes in the finite element solution of 2D viscous flows problems involving heat transfer combined with surface tension effects. We compare the efficiency of the control strategies for timestep selection with another heuristic adaptive stepsize selection scheme.[2] We also investigate the use of the non-dimensional kinetic energy to improve the timestep selection when coordinated with the convergence rate control of the nonlinear iterations.

We consider the transient flow of a viscous incompressible fluid as described by the Navier-Stokes equations coupled to the heat transfer equation. The present algorithm employs a decoupled scheme, where the momentum and continuity equations are solved first, in each timestep, lagging the temperature in the forcing term. Then, the heat transfer equation is solved with the computed velocities as input. The finite element

flow formulation is based on a penalty Galerkin method to enforce the incompressibility constraint, and the heat equation utilizes a Galerkin approach.

In the next section we briefly state the class of coupled viscous flow and heat transfer problems under investigation, the finite element formulation and the solution approach. Then, we describe two timestep control algorithms based on controlling either accuracy or the convergence rate of the successive iterations. Next, results of the classic Rayleigh-Benard problem and Rayleigh-Benard-Marangoni problem are compared for fixed timestep, an adaptive timestep scheme found in the literature and our control approaches.

2 FORMULATION AND APPROXIMATION

2.1 Governing Equations

We consider the transient flow of a viscous incompressible fluid as described by the Navier-Stokes equations coupled to the energy equation. Of particular interest in the present work are 2-D Rayleigh-Benard flows and Rayleigh-Benard-Marangoni flows. The present algorithm employs a decoupled scheme, where the Navier-Stokes equations are solved first, in each timestep, lagging the temperature in the forcing term. Then, the energy equation is solved with the computed velocities as input. A single timestep for all equations is adaptively chosen using the control strategies described in the next section. The finite element flow formulation is based on a penalty Galerkin method to enforce the incompressibility constraint. The heat transfer equation employs a Galerkin approach.

The Navier Stokes equations for viscous flow of incompressible fluids may be written as

$$\frac{\partial \mathbf{u}}{\partial t} + \mathbf{u} \cdot \nabla \mathbf{u} - \nu \Delta \mathbf{u} + \frac{1}{\rho} \boldsymbol{\nabla} p = \beta_T (T - T_0)\, \mathbf{g} \quad \text{in } \Omega \tag{1}$$

$$\boldsymbol{\nabla} \cdot \mathbf{u} = 0 \quad \text{in } \Omega \tag{2}$$

where Ω is the flow domain, $\mathbf{u}$ is the velocity, p is the pressure, T is the temperature, ν is the kinematic viscosity, ρ is the density, β_t is the thermal volume expansion, $\mathbf{g}$ is the gravity vector, and T_0 is the reference temperature. We assume that there is no slip boundary conditions at the solid walls $\partial\Omega_1$, i.e., $\mathbf{u} = \mathbf{u_w}$ where $\mathbf{u_w}$ is the specified wall boundary velocity. The Marangoni problem involves a shear stress boundary in the free surface $\partial\Omega_2$. The surface stress, τ_{fb}, tangent to the free boundary is equal to the gradient in the surface tension σ,

$$\tau_{fb} = \mu \frac{\partial u}{\partial y} = \sigma_T \frac{\partial T}{\partial x} \tag{3}$$

where μ is the viscosity, and $\sigma_T = \frac{\partial \sigma}{\partial T}$ is determined empirically for a given fluid. The surface tension varies linearly with temperature, and we assume here that σ_T is constant

for a given fluid. The temperature of the fluid is governed by the energy transport equation for negligible viscous dissipation

$$\rho c_p \frac{\partial T}{\partial t} + \rho c_p \mathbf{u} \cdot \nabla T - \nabla \cdot (k \nabla T) = 0 \quad \text{in } \Omega \tag{4}$$

where $\mathbf{u}$ is the velocity, c_p is the specific heat, and k is the thermal conductivity. The boundary conditions are as follows: $T = T_1(x, y)$ (isothermal boundary) or $\frac{\partial T}{\partial n} = 0$ (adiabatic boundary) on the solid walls $\partial\Omega_1$, and mixed conditions $\alpha \frac{\partial T}{\partial n} = h_c(T - T_e)$ (Robin) on the free surface $\partial\Omega_2$, where $\alpha_T = \frac{k}{\rho c_p}$ is the thermal diffusivity, h_c is the heat transfer coefficient for the medium, and T_e is the exterior temperature.

2.2 Finite Element Formulations

Introducing a finite element discretization and basis on Ω_h, the direct approximation of the penalized variational formulation of the Navier-Stokes equations[8,9] reduces to: for $\epsilon > 0$, find $\mathbf{u}_h^\epsilon \in V^h$ satisfying the initial condition with $\mathbf{u}_h^\epsilon = \mathbf{u}_w$ on $\partial\Omega_1$ such that

$$\begin{aligned} \int_{\Omega_h} \frac{\partial \mathbf{u}_h^\epsilon}{\partial t} \cdot \mathbf{w}_h \, dx \;+\; & \int_{\Omega_h} \mathbf{u}_h^\epsilon \cdot \nabla \mathbf{u}_h^\epsilon \cdot \mathbf{w}_h \, dx \;+ \int_{\Omega_h} \nu \nabla \mathbf{u}_h^\epsilon : \nabla \mathbf{w}_h \, dx \\ + \; & \frac{1}{\epsilon} \mathbf{I}(\nabla \cdot \mathbf{u}_h^\epsilon)(\nabla \cdot \mathbf{w}_h) \, dx \\ = \; & \int_{\partial\Omega_{2h}} \sigma_T \nabla T \cdot \mathbf{w}_h \, ds \\ + \; & \int_{\Omega_h} \beta_T (T - T_0) \, \mathbf{g} \cdot \mathbf{w}_h \, dx \quad \text{for all } \mathbf{w}_h \in V^h \end{aligned} \tag{5}$$

where $\mathbf{I}$ denotes reduced numerical integration, and ϵ is the penalty parameter. This leads to the following non-linear semidiscrete system of ordinary differential equations

$$\mathbf{M} \frac{d\mathbf{U}}{dt} + \mathbf{s}(\mathbf{U}) + \nu \mathbf{A}\mathbf{U} + \frac{1}{\epsilon} \mathbf{B}\mathbf{U} = \mathbf{b}(\mathbf{T}) \tag{6}$$

To advance the solution from a specified initial state, we integrate implicitly using a standard θ method, so that at timestep (t_n, t_{n+1}):

$$\begin{aligned} \frac{\mathbf{M}(\mathbf{U}^{n+1} - \mathbf{U}^n)}{\Delta t} \;+\; & \theta \left[\mathbf{s}(\mathbf{U}^{n+1}) + \nu \mathbf{A}\mathbf{U}^{n+1} + \frac{1}{\epsilon} \mathbf{B}\mathbf{U}^{n+1} \right] \\ + \; & (1 - \theta) \left[\mathbf{s}(\mathbf{U}^n) + \nu \mathbf{A}\mathbf{U}^n + \frac{1}{\epsilon} \mathbf{B}\mathbf{U}^n \right] = \theta \mathbf{G}^n + (1 - \theta) G^{n+1} \end{aligned} \tag{7}$$

where $\mathbf{G} = \mathbf{b}(\mathbf{T})$ is evaluated using the previous temperature iterate. Here $\theta = 1/2$ which corresponds to the familiar Crank-Nicolson integrator. The nonlinearity resides in the convective term $\mathbf{s}(\mathbf{U})$, which is linearized by successive approximations, $\mathbf{s}(\mathbf{U}) \approx$

$\mathbf{s}(\mathbf{U}_{k-1})\mathbf{U}_k = \int_{\Omega_h} \mathbf{u}_h^{k-1} \cdot \nabla \mathbf{u}_h^k \cdot \mathbf{v}_h \, dx$, with initial iterates given by the solution at the previous step. Hence we have to solve a sequence of linear systems at each timestep. Solutions of the resulting linear systems are obtained using a frontal solver.

To find approximate solutions for the transport problem corresponding to (4), we use a traditional Galerkin finite element formulation. A weak variational statement may be obtained by integration by parts of the diffusion term in a standard residual formulation, and then using the Gauss divergent theorem. Assuming that convective and diffusive effects are of same order, we may construct a semidiscrete Galerkin finite element method introducing a spatial discretization and an appropriate finite element space for the admissible functions. The finite element problem is to find $T_h \in {H_0}^h$ satisfying the initial condition such that

$$\int_{\Omega_h} (\frac{\partial T_h}{\partial t}\omega_h + \mathbf{u} \cdot \nabla T_h \, \omega_h + \alpha \nabla T_h \cdot \nabla \omega_h) \, dx = 0 \tag{8}$$

for all $\omega_h \in {H_0}^h$, where $\alpha = \frac{k}{\rho c_p}$ is the thermal diffusivity. The resulting semi-discrete ODE system for the nodal vector $\mathbf{T}$ has the form

$$\mathbf{N}\frac{d\mathbf{T}}{dt} + \mathbf{C}(\mathbf{u})\,\mathbf{T} + \mathbf{D}\,\mathbf{T} = 0, \tag{9}$$

which is integrated implicitly using the standard θ method. This leads to the linear algebraic system

$$\begin{aligned} \frac{\mathbf{N}(\mathbf{T}^{n+1} - \mathbf{T}^n)}{\Delta t} &+ \theta \left[\mathbf{C}(\mathbf{u})\mathbf{T}^{n+1} + \mathbf{D}\mathbf{T}^{n+1}\right] \\ &+ (1-\theta)\left[\mathbf{C}(\mathbf{u})\mathbf{T}^{n} + \mathbf{D}\mathbf{T}^{n}\right] = 0 \end{aligned} \tag{10}$$

to be solved for each timestep Δt. Here n denotes the timestep index. We use the Crank-Nicolson scheme, $\theta = 1/2$, and a frontal solver to find solutions of the resulting linear systems. In the next section we describe two possible strategies for timestep selection based on controlling accuracy or the convergence rate of the successive iterations.

3 CONTROL ALGORITHMS

Many studies have been made to improve stepsize selection in numerical integration of ordinary differential equations; e.g. in the finite element field we can find timestep selection strategies based on heuristic rules such as in Winget and Hughes[2] for transient heat conduction. Gustafsson and Soderlind[10] and Hairer and Wanner[11] viewed the problem of automatic timestep selection as examples of feedback control problems. This approach was used by Coutinho and Alves[3] in their work on finite element simulation of miscible displacements in porous media. Valli, Coutinho and Carey develop adaptive stepsize control strategies in finite element simulation of nonlinear flow and reactive transport,[4] and coupled viscous flow and heat transfer.[5,6]

Most timestep schemes are based on controlling accuracy as determined by truncation error estimates (e.g. Prediction-Modification-Correction). The objective of timestep selection is to minimize the computational effort to construct an approximate solution of a given problem in accordance with a desired accuracy. Hairer and Wanner[11] showed that stepsize selection can be viewed as an automatic control problem with a PID controller defined as

$$\triangle t_{n+1} = (\frac{e_{n-1}}{e_n})^{k_P} (\frac{tol}{e_n})^{k_I} (\frac{{e_{n-1}}^2}{e_n e_{n-2}})^{k_D} \ \triangle t_n, \tag{11}$$

where tol is some input tolerance, e_n is the measure of the change of the quantities of interest in time t_n, and k_P, k_I and k_D are the PID parameters. An estimate of the solution change is compared with the specified accuracy requirement, and the result is fed back to calculate the new time step. The controller tries to select the stepsize such that e_n comes as close as possible to the input tolerance, tol, along a smooth curve, see Figure 1.

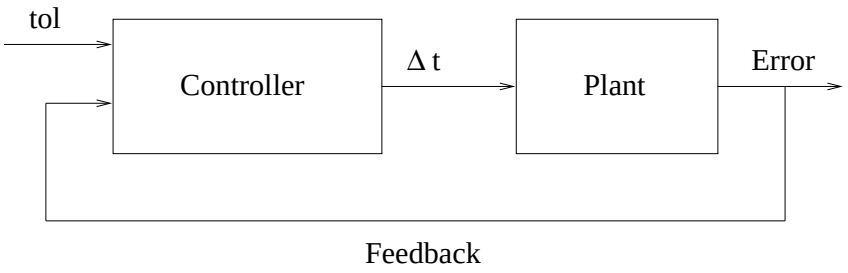

Figure 1: Stepsize selection viewed as a control problem.

In the present work, we consider two different ways to define the measure of the change over a timestep of the quantities of interest, e_n. First, we use the changes in nodal velocities and temperature to compute e_n taking,

$$e_n = \max\left(e_u, e_T\right) \tag{12}$$

where

$$e_u = \frac{e_u^*}{\mathrm{tol}_u} \qquad e_u^* = \frac{\|\mathbf{u}^{n+1} - \mathbf{u}^n\|}{\|\mathbf{u}^{n+1}\|} \tag{13}$$

$$e_T = \frac{e_T^*}{\mathrm{tol}_T} \qquad e_T^* = \frac{\|\mathbf{T}^{n+1} - \mathbf{T}^n\|}{\|\mathbf{T}^{n+1}\|} \tag{14}$$

where tol_u and tol_T are user supplied tolerances corresponding to the normalized changes in velocities and temperature, respectively. Second, we define e_n computing changes in the nondimensional kinetic energy given by $K = \int_\Omega \frac{({u^*}^2 + {v^*}^2)}{2} dxdy$, where u^* and v^* are the nondimensional velocities components. Now e_n is defined by

$$e_n = \frac{e_K^*}{\mathrm{tol}_K}, \qquad e_K^* = \frac{|K^{n+1} - K^n|}{|K^{n+1}|} \tag{15}$$

where tol_K is a given tolerance. The nondimensional kinetic energy is a suitable parameter for monitoring the behavior of the fluid as time progresses. For example, we can say that the steady-state occurs when the kinetic energy at two different time steps reaches a difference less than an input tolerance.

In the numerical integration of the Navier-Stokes by the implicit Crank-Nicolson method, a system of nonlinear equations has to be solved at every step. In the present work we use fixed-point iterations given by successive approximations. The convergence rate of the iterative method depends on the stepsize, and the computational efficiency of the method can be measured by the total number of successive iterations to obtain the final solution. To improve efficiency, diminishing computational costs, it is necessary to control the convergence rate of the fixed point iterations.

Gustafsson and Söderlind[7] establish a model for controlling the convergence rate of the iterative method that relates the convergence rate to the stepsize. Assuming that the stepsize is limited by the convergence rate of nonlinear iterations, the new stepsize should be chosen as

$$\Delta t_{n+1} = \frac{\alpha_{ref}}{\alpha}\,\Delta t_n \tag{16}$$

where α_{ref} is a reference rate of convergence and α is an estimated rate of convergence. Now the controller tries to keep the estimated convergence rate as close as possible of a reference value. We must find which is the convergence rate, α_{ref}, the controller aim for to give the most efficient integration. In general, any value $0.2 < \alpha_{ref} < 0.4$ would be acceptable, and $\alpha_{ref} \approx 0.2$ gives performance near to optimal.[7] The estimated rate of convergence is calculated using three consecutive iterates, $\mathbf{u}_{n-1}$, $\mathbf{u}_n$, and $\mathbf{u}_{n+1}$, as follows

$$\alpha = \max \alpha_n = \max_n \frac{\|\mathbf{u}_{n+1} - \mathbf{u}_n\|}{\|\mathbf{u}_n - \mathbf{u}_{n-1}\|}. \tag{17}$$

It is necessary to coordinate the convergence control algorithm (16) with the stepsize control strategy (11) so that efficiency is maintained.

We propose two timestep control algorithms based on controlling accuracy or the convergence rate of the successive iterations. The first control uses only the PID control for timestep selection, (11), with changes in velocities and temperature. The **Control 1** is defined by

$$\triangle t_{n+1} = \left(\frac{e_{n-1}}{e_n}\right)^{k_P} \left(\frac{tol}{e_n}\right)^{k_I} \left(\frac{{e_{n-1}}^2}{e_n e_{n-2}}\right)^{k_D} \triangle t_n \tag{18}$$

where

$$e_n = \max\,(e_u, e_T), \tag{19}$$

and Δt_{n+1} represents the new timestep size. The definition of e_u and e_T is given by equations (13) and (14). In the second control, the size of the timestep is limited by the changes

in the kinetic energy or by the rate of convergence of the successive approximations. We take the minimum between the two values. The **Control 2** is given by

$$\Delta t_{n+1} = \min(\Delta t_\alpha, \Delta t_r), \tag{20}$$

where

$$\Delta t_\alpha = \frac{\alpha_{ref}}{\alpha}\,\Delta t_n \tag{21}$$

$$\triangle t_r = \left(\frac{e_{n-1}}{e_n}\right)^{k_P}\left(\frac{tol}{e_n}\right)^{k_I}\left(\frac{{e_{n-1}}^2}{e_n e_{n-2}}\right)^{k_D}\triangle t_n \tag{22}$$

with

$$e_n = \frac{e_K^*}{\mathrm{tol}_K}, \qquad e_K^* = \frac{|K^{n+1} - K^n|}{|K^{n+1}|}. \tag{23}$$

Experimental studies will be given in the next section showing the efficiency of the two controls, (18) and (20). Comparative studies between the two controls will also be carried out for a representative test problem for Rayleigh-Benard-Marangoni flows.

4 NUMERICAL RESULTS AND DISCUSSIONS

Buoyancy and thermocapillary surface traction due to temperature gradients on the free surface provide the dominant forces driving 2-D Rayleigh-Benard-Marangoni flows. Buoyancy enters the momentum equation as a body force term, and the effect of the thermocapillary surface tensions enters as an applied shear stress. The dimensionless equations describing the Rayleigh-Benard-Marangoni flows are

$$\frac{\partial \mathbf{u}}{\partial t} + \mathbf{u}\cdot\nabla\mathbf{u} - \Delta\mathbf{u} + \boldsymbol{\nabla} p = \frac{Ra}{Pr} T\mathbf{g} \tag{24}$$

$$\boldsymbol{\nabla}\cdot\mathbf{u} = 0 \tag{25}$$

$$\frac{\partial T}{\partial t} + \mathbf{u}\cdot\nabla T - \frac{1}{Pr}\nabla^2 T = 0 \tag{26}$$

where $Ra = \frac{\beta_T \Delta T g L^3}{\nu\alpha}$ is the Rayleigh number, $Pr = \frac{\nu}{\alpha}$ is the Prandtl number, ΔT is the temperature difference for flows with heated or cooled walls and L is a characteristic length scale of the flow. The equations were scaled using the following dimensionless variables: $x^* = \frac{x}{L}$, $y^* = \frac{y}{L}$, $t^* = \frac{t\nu}{L^2}$, $u^* = \frac{uL}{\nu}$, $v^* = \frac{vL}{\nu}$, $T^* = \frac{T-T_0}{\Delta T}$ and $p^* = (\frac{p}{\rho})\frac{L^2}{\nu^2}$. For convenience, we drop the superscript *. The non-dimensional boundary condition on the free surface becomes

$$\frac{\partial u}{\partial y} = \frac{Ma}{Pr}\frac{\partial T}{\partial x}, \tag{27}$$

where $Ma = \frac{\sigma_T \Delta T L}{\rho \nu \alpha}$ is the Marangoni number. Equations (24), (25), (26) and (27) constitute a coupled system of equations to be solved for velocity, pressure and temperature using the numerical scheme described in section 2.2.

The first case studied involves natural convection in a unit square with temperatures $T = 1$, $T = 0$ on the left and right walls respectively, adiabatic top and bottom wall (no free surface), with $Pr = 0.71$ and different Rayleigh numbers, Ra, of 10^3, 10^4 and 10^5. The computed Nusselt number at the left wall,

$$Nu_0 = \int_0^1 q dy, \tag{28}$$

where q is the heat flux, and the stream function at the midpoint, ψ_{mid}, are compared to benchmark computations.[12] It is believed that this benchmark solution is in error by no more than 1 per cent for all Rayleigh numbers. We compare approximate solutions using fixed timestep sizes, Control 1, Control 2, the Winget and Hughes approach and the benchmark solution.

The approximate velocities and temperature are calculated using 9-node isoparametric quadrilaterals elements in a uniform mesh of 16×16 elements at $Ra = 10^3$, 10^4 and 32×32 elements at $Ra = 10^5$. We assume that the steady-state occurs when the kinetic energy at two different time steps reaches a relative difference less than a given tolerance, tol_{st}. The initial timestep size in all cases is chosen to have convergence of the successive iterations at the beginning of the process. If we start with a timestep size greater than the initial timestep defined below, the successive approximation iterations failed to converge after a few time steps. The results are shown in Table 1.

Table 1: Comparison of specific results to benchmark case

	Fixed Δt		Control 1		Control 2		Winget&Hughes		Benchmark	
Ra	Nu_0	ψ_{mid}	Nu_0	ψ_{mid}	Nu_0	ψ_{mid}	Nu_0	ψ_{mid}	Nu_0	ψ_{mid}
10^3	1.118	1.175	1.119	1.175	1.117	1.174	1.119	1.175	1.117	1.174
10^4	2.255	5.067	2.236	5.077	2.246	5.064	2.249	5.066	2.238	5.071
10^5	4.550	9.134	4.518	9.036	4.553	9.120	4.503	8.925	4.509	9.111

Table 2 contains the percentage relative differences between the values calculated by each case studied and the corresponding values of the benchmark solution for the different Rayleigh numbers. The results are in good agreement for all the cases, with percentage errors no more than 1% in all quantities for Control 1 and Control 2, see Table 2. However, observe that the differences increase as Ra increases due to the growing difficulty of the problem. The Winget and Hughes approach also produces good results with percentage errors no more than 2% in all quantities.

Table 2: Percentage errors

	Fixed Δt		Control 1		Control 2		Winget&Hughes	
Ra	Nu_0	ψ_{mid}	Nu_0	ψ_{mid}	Nu_0	ψ_{mid}	Nu_0	ψ_{mid}
10^3	0.1	0.1	0.2	0.1	0.0	0.0	0.2	0.1
10^4	0.8	0.1	0.1	0.1	0.4	0.1	0.5	0.1
10^5	0.9	0.3	0.2	0.8	1.0	0.1	0.1	2.0

Now we compare the computational effort to calculate the solution for each case studied. The computational effort is measured by the total number of successive approximations needed to calculate the velocity field using one of the approaches divided by the number of successive approximations obtained using a fixed timestep size. For each case, we calculate the number of time iterations, $ntstep$, the number of rejected steps, $nrejec$, the total number of successive approximations, nsa, and the computational effort, c_{effort}. The PID parameters in all cases are $k_p = 0.075$, $k_i = 0.175$ and $k_d = 0.01$.[4–6]

The results for $Ra = 10^3$ are shown in Table 3. We start with a minimum timestep size of 0.01, and we allow a maximum timestep size of 0.1. We define a tolerance of 0.1 for changes in nodal velocities and temperature. The tolerance corresponding to the normalized changes in kinetic energy is equal to one. The reference rate of convergence is equal to 0.2. We assume that the steady-state solution is reached when $tol_{st} = 10^{-4}$. We can observe in Table 3 that the number of successive approximations necessary to calculate the approximate solutions was reduced for all approaches. However, Control 2 presented the best results. We obtain the solution with 24 successive iterations using Control 2, and we need 64 iterations with the fixed timestep. Thus, we are able to calculate the solution 2.4 times faster using the Control 2 without any significant loss of accuracy. For Control 2, the choice of the timestep is dominated by the changes in the kinetic energy in all iterations.

Table 3: Computational effort for the natural convection problem, $Ra = 10^3$.

$Ra = 10^3$	$ntstep$	$nrejec$	nsa	c_{effort}
Fixed Δt	24	0	58	1
Control 1	11	0	32	0.55
Control 2	8	0	24	0.41
Winget&Hughes	15	0	41	0.71

Figure 2 shows the timestep size against time and time against the number of successive approximations using Control 1, Control 2 and the Winget and Hughes approach for $Ra = 10^3$. In this example the kinetic energy is the most suitable parameter to choose

the timestep, since Control 2 gives the best result. It is worthwhile noting also that Control 2 begins to act before any other approach and, after a few steps, provides a timestep equal to the maximum stepsize allowed, 0.1.

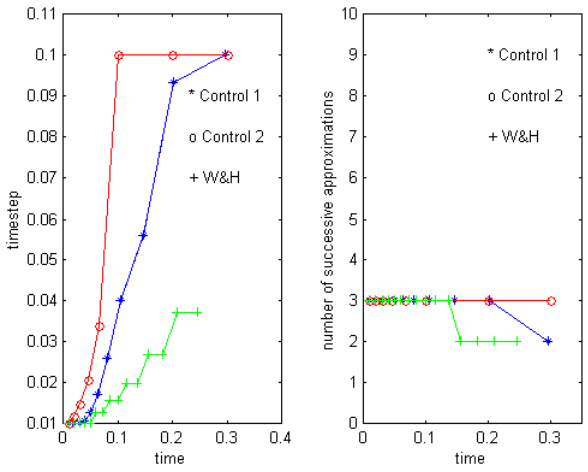

Figure 2: Timestep variation (left) and number of successive approximations (right) using Control 1, Control 2 and the Winget and Hughes approach for $Ra = 10^3$.

Table 4 shows the results for $Ra = 10^4$. We start with a minimum timestep of 0.01, and we allow a maximum timestep size of 0.01. We define tolerances of 0.2, 0.1 and 0.5 for changes in nodal velocities, temperature and kinetic energy, respectively. The reference rate of convergence is equal to 0.19. We establish that the steady-state occurs when $tol_{st} = 10^{-3}$. Here we also improve efficiency for all approaches, reducing the number of successive approximations necessary to calculate the approximate solutions. Control 1 and Control 2 are equivalent in terms of efficiency. The choice of the timestep in Control 2 is dominated by the convergence rate of the successive iterations, with only two time iterations limited by the changes in the kinetic energy. Control 1, which is based on controlling accuracy, gives timestep sizes larger than the ones calculated by Control 2, see Figure 3.

Table 4: Computational effort for the natural convection problem, $Ra = 10^4$.

$Ra = 10^4$	$ntstep$	$nrejec$	nsa	c_{effort}
Fixed Δt	14	0	56	1
Control 1	10	0	47	0.84
Control 2	10	0	45	0.80
Winget&Hughes	12	0	52	0.93

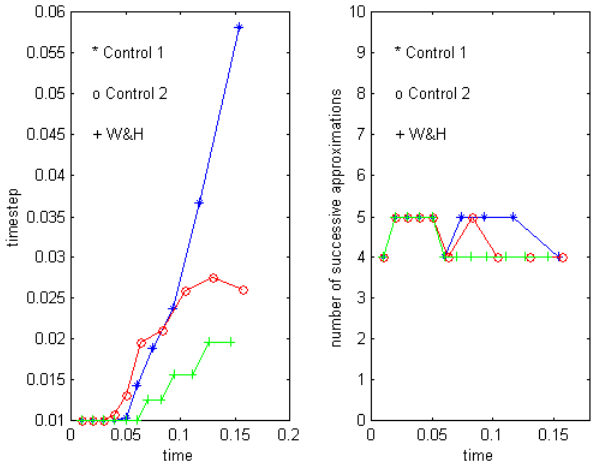

Figure 3: Timestep variation (left) and number of successive approximations (right) using Control 1, Control 2 and the Winget and Hughes approach for $Ra = 10^4$.

Table 5 shows the results for $Ra = 10^5$. We start with a minimum timestep size of 0.001, and we allow a maximum timestep size of 0.1. We define a tolerance of 0.1 for changes in nodal velocities and temperature. The tolerance corresponding to the normalized changes in kinetic energy is equal to one. The reference rate of convergence is equal to 0.25. We establish that the steady-state occurs when $tol_{st} = 10^{-3}$. Now, Control 2 is dominated by the changes in the kinetic energy, with only 4 iterations calculated according to the the convergence rate of the successive iterations. All approaches reduce the number of successive approximations to obtain the solution, but Control 2 gives the best result. The total number of successive approximations obtained by Control 1 can be reduced if we define large tolerances for changes in nodal velocities and temperature. However, the results will loose accuracy, yielding errors greater than 1% as the case of the Winget and Hughes approach (see Table 2).

Table 5: Computational effort for the natural convection problem, $Ra = 10^5$.

$Ra = 10^5$	$ntstep$	$nrejec$	nsa	c_{effort}
Fixed Δt	108	0	363	1
Control 1	48	5	260	0.72
Control 2	39	0	189	0.52
Winget&Hughes	48	3	244	0.67

Figure 4 shows the timestep size against time and the time against the number of successive approximations using Control 1, Control 2 and the Winget and Hughes approach for $Ra = 10^5$. Since the size of the timestep increases significantly when time progress

for Control 1 and the Winget and Hughes approach, the number of successive iterations to obtain convergence of the nonlinear process at each corresponding time also increases. This fact is responsible by the larger number of successive iterations calculated by these two approaches when compared with Control 2. Figure 5 shows the nondimensional kinetic energy for $Ra = 10^3$, $Ra = 10^4$ and $Ra = 10^5$. The kinetic energy is also a suitable parameter to monitor convergence to steady-state. The stream function contours and temperature contours are shown in Figure 6.

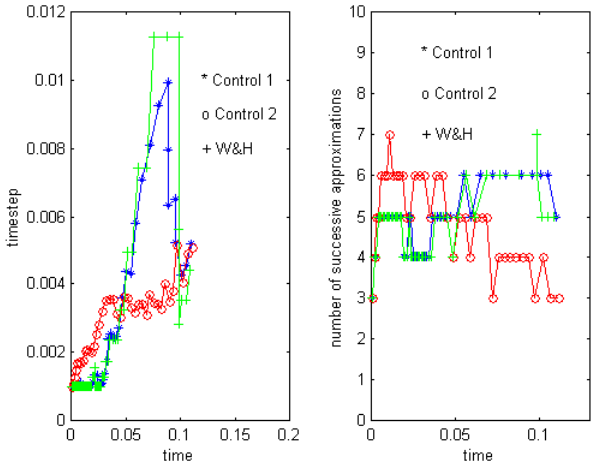

Figure 4: Timestep variation (left) and number of successive approximations (right) using Control 1, Control 2 and the Winget and Hughes approach for $Ra = 10^5$.

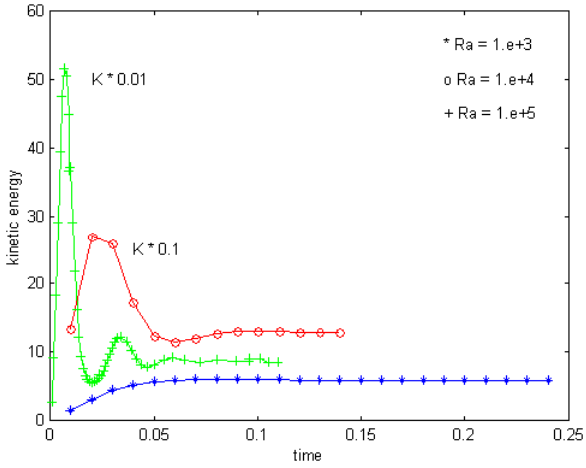

Figure 5: Nondimensional kinetic energy plotted as a function of time for $Ra = 10^3$, $Ra = 10^4$ and $Ra = 10^5$.

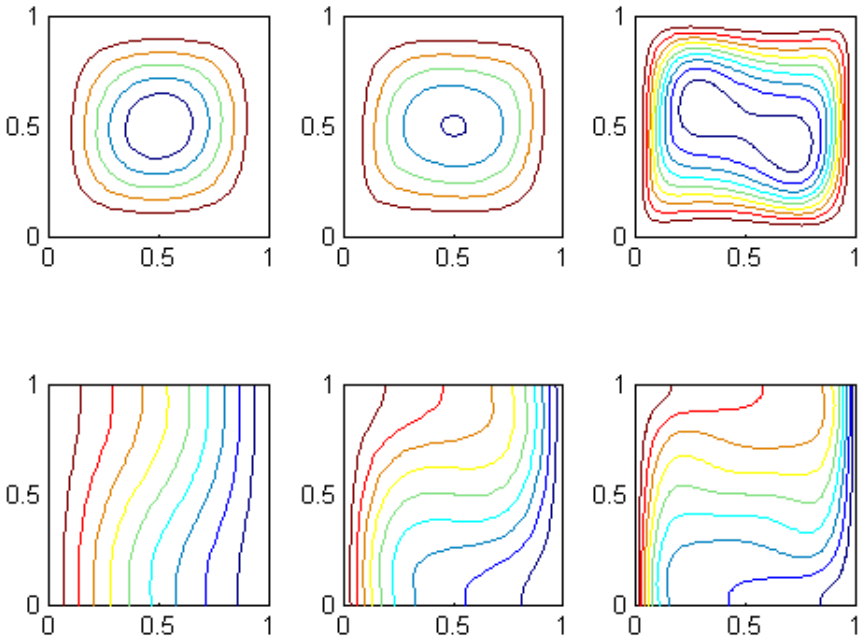

Figure 6: Stream functions contours (top) and temperature contours (bottom) for $Ra = 10^3$, $Ra = 10^4$ and $Ra = 10^5$.

The second numerical experiment involves buoyancy forces due to temperature gradients and thermocapillary forces caused by gradients in the surface tension. The flow domain and boundary conditions are the same as the first example, except that the top is now a flat free surface. The Rayleigh number is 10^3, the Prandtl number is 0.71, and the problem is solved at different Marangoni numbers. The approximate steady-state velocities and temperature are calculated using biquadratic elements in a uniform mesh with size $h = \frac{1}{16}$. Here we assume that the steady-state occurs when $\|\mathbf{u}^{n+1} - \mathbf{u}^n\| < \tau_u \|\mathbf{u}^{n+1}\|$ and $\|\mathbf{T}^{n+1} - \mathbf{T}^n\| < \tau_T \|\mathbf{T}^{n+1}\|$, where n denotes the timestep index, $\|\cdot\|$ denotes Euclidean norm, and τ_u and τ_T are input tolerances.

First, we find solutions at M = -1, -100 and -1000 (see Figure 7). At M = -1, the effect of the surface tension is small and the streamlines are roughly circular. The solution is similar in structure to the classic buoyancy driven flow studied in the first example, Figure 6. At M = -100, the effect of the thermocapillary force at the free surface is more pronounced. The streamlines are concentrated near the top boundary. At M = -1000, the flow is being strongly driven at the top boundary as seen in similar experiments presented by Zebib, Homsy and Meiburg.[13]

Now, we consider the case of a fluid where the surface tension acts in the direction contrary to the flow. Figure 8 shows the stream function contours for $M = 10$ and $M = 100$. The contours at $M = 10$ look similar to the solution at M = -1 due to the small

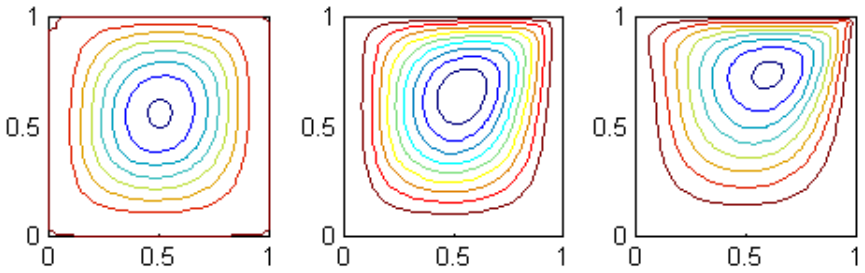

Figure 7: Stream function contours for $Ma = -1$, $Ma = -100$ and $Ma = -1000$.

thermocapillary effect. At $M = 100$, the surface tension effect is strong enough to reverse the flow on the top surface and two cells are formed.

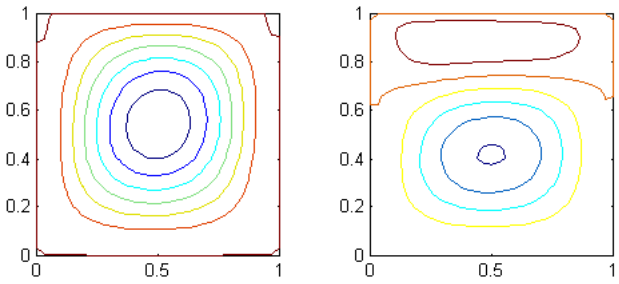

Figure 8: Stream function contours for $Ma = 10$ and $Ma = 100$

To study the behavior of the PID timestep selection in the second problem, we select the case where M = -100. The steady-state solution is obtained at $\tau_u = 10^{-3}$ and $\tau_T = 10^{-4}$. We start with a minimum timestep size of 0.001, and we allow a maximum timestep of 0.1. Solutions are obtained with tolerances of 0.2 and 0.1 for changes in nodal velocities and temperature, respectively. The tolerance corresponding to the normalized changes in kinetic energy is equal to one. The reference rate of convergence is equal to 0.2. As we can see in Table 6, we obtain the solutions with 57 successive approximation iterations using Control 2. With a fixed timestep size of 0.001, we need 272 iterations. Thus, the solutions are obtained 4.8 times faster using Control 2. Here, the choice of the timestep in Control 2 is dominated by the changes in the kinetic energy, with only three time iterations limited by the changes in the convergence rate of the successive iterations.

Figure 9 shows the timestep variation and the number of successive approximations against time using Control 1, Control 2 and the Winget and Hughes approach. We can observe that Control 1 yields a smoother sequence of time steps than the Winget and Hughes approach. However, these two approaches are equivalent in terms of efficiency.

Table 6: Computational effort for the Rayleigh-Benard-Marangoni problem, Pr = 0.71, Ra = 1000 and Ma = -100 in a unit square.

Case	$ntstep$	$nrejec$	nsa	c_{effort}
Fixed Δt	118	0	272	1
Control 1	23	0	75	0.28
Control 2	13	0	57	0.21
Winget&Hughes	25	0	80	0.29

Control 2 calculates the solutions with the smallest computational effort. Figure 10 shows the time evolution of the nondimensional kinetic energy for Pr = 0.71, Ra = 1000 and Ma = -100. Note that the kinetic energy presents smooth oscillations, damped as the solution progresses towards the steady-state.

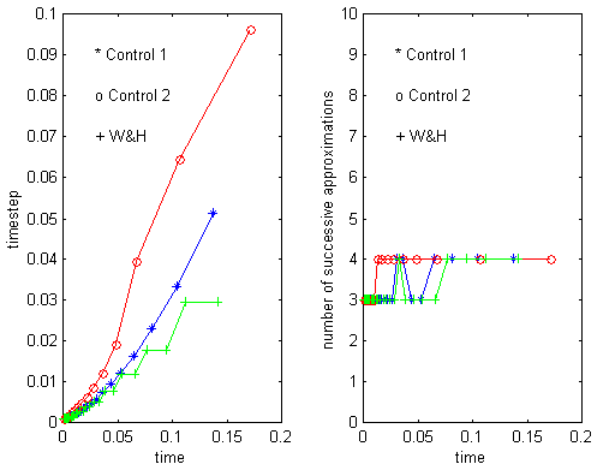

Figure 9: Timestep variation (left) and number of successive approximations (right) using Control 1, Control 2 and the Winget and Hughes approach for Pr = 0.71, Ra = 1000 and Ma = -100 in a unit square

5 CONCLUSIONS

In this study, it is shown that, using control strategies for timestep selection and convergence rate improvement of nonlinear iterative processes, the computational efficiency of finite element solutions of 2D viscous flows problems involving heat transfer combined with surface tension effects can be improved. It is presented comparison results on the study of representative Rayleigh-Benard and Rayleigh-Benard-Marangoni problems using a fixed timestep, an adaptive timestep scheme from the literature and our two control approaches. It is also investigated the use of the non-dimensional kinetic energy to im-

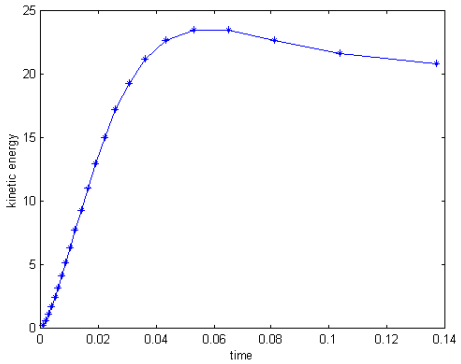

Figure 10: Nondimensional kinetic energy plotted as a function of time for Pr = 0.71, Ra = 1000 and Ma = -100 in a unit square

prove the timestep selection when coordinated with the convergence rate control of the nonlinear iterations.

Based on numerical studies of representative Rayleigh-Benard and Rayleigh-Benard-Marangoni problems, it is concluded that we find approximate solutions with a smaller number of steps without any significant loss of accuracy. In addition, the controllers also produce a smooth variation of timestep, suggesting that a robust control algorithm is possible. Further, the control strategy that maintains the desired solution accuracy by adjusting the timestep size to account for changes in the kinetic energy or by the rate of convergence of the successive approximations showed the best results in all cases studied here.

REFERENCES

[1] G.F. Carey, C. Harlé, R. Mclay, and S. Swift. MPP solution of Rayleigh-Benard-Marangoni flows. In *Supercomputing 97*, pages 1–13, San Jose, CA, (1997).

[2] J.M. Winget and T.J.R. Hughes. Solution algorithms for nonlinear transient heat conduction analysis employing element-by-element iterative strategies. *Comp. Meth. Appl. Mech. and Eng.*, **52**, 711–815 (1985).

[3] A.L.G.A. Coutinho and J.L.D. Alves. Parallel finite element simulation of miscible displacements in porous media. *SPE Journal*, **4**(1), 487–500 (1996).

[4] A.M.P. Valli, G.F. Carey, and A.L.G.A. Coutinho. Finite element simulation and control of nonlinear flow and reactive transport. In *Proc. 10th Int. Conf. Finite Element in Fluids*, pages 450–455, Tucson, Arizona, (1998).

[5] A.M.P. Valli, A.L.G.A. Coutinho, and G.F. Carey. Adaptive control for time step selection in finite element simulation of coupled viscous flow and heat transfer. In *European Conference on Computational Mechanics*, Munchen, Germany, (August 1999).

[6] A.M.P. Valli, A.L.G.A. Coutinho, and G.F. Carey. Adaptive stepsize control strategies in finite element simulation of 2D Rayleigh-Benard-Marangoni flows. In *15th*

Brazilian Congress on Mechanical Sciences, Águas de Lindóia, SP, Brazil, (November 1999).

[7] K. Gustafsson and G. Söderlind. Control strategies for the iterative solution of nonlinear equations in ODE solvers. *SIAM J. Sci. Comput.*, **18**(1), 23–40 (1997).

[8] G.F. Carey and J.T. Oden. *Finite Elements: Fluid Mechanics*, volume 6. Prentice–Hall, Englewood Cliffs, NJ, (1986).

[9] G.F. Carey and R. Krishnan. Penalty finite element methods for the Navier–Stokes equations. *Comput. Meths. Appl. Mech. Engrg.*, **42**, 183–224 (1984).

[10] K. Gustafsson, M. Lundh, and G. Söderlind. A PI stepsize control for the numerical solution for ordinary differential equations. *BIT*, **28**, 270–287 (1988).

[11] E. Hairer and G. Wanner. *Solving Ordinary Differential Equations II: Stiff and Differential-Algebraic Problems*. Springer–Verlag, (1993).

[12] G.De Vahl Davis. Natural convection in a square cavity: A comparison exercise. *Int.J.Num.Meth.Fluids*, **3**, 227–248 (1983).

[13] A. Zebib, G.M. Homsy, and E. Meiburg. High Marangoni number convection in a square cavity. *Phys. Fluids*, **28**(12), 3467–3476 (1985).